Advances in Engineering Software 52 (2012) 30–43

Contents lists available at SciVerse ScienceDirect

Advances in Engineering Software

journal homepage: www.elsevier.com/locate/advengsoft

Static analysis of functionally graded sandwich plates according to a hyperbolic theory considering Zig-Zag and warping effects

A.M.A. Neves [a], A.J.M. Ferreira [a,*], E. Carrera [b], M. Cinefra [b], R.M.N. Jorge [a], C.M.M. Soares [c]

[a] Departamento de Engenharia Mecânica, Faculdade de Engenharia, Universidade do Porto, Rua Dr. Roberto Frias, 4200-465 Porto, Portugal
[b] Departament of Aeronautics and Aerospace Engineering, Politecnico di Torino, Corso Duca degli Abruzzi, 24, 10129 Torino, Italy
[c] Instituto Superior Técnico, Av. Rovisco Pais, Lisboa, Portugal

ARTICLE INFO

Article history:
Received 27 December 2011
Received in revised form 18 April 2012
Accepted 23 May 2012
Available online 7 July 2012

Keywords:
Sandwich plates
Plates
Functionally graded materials
Meshless methods
Higher-order theories
Composites

ABSTRACT

In this paper, a variation of Murakami's Zig-Zag theory is proposed for the analysis of functionally graded plates. The new theory includes a hyperbolic sine term for the in-plane displacements expansion and accounts for through-the-thickness deformation, by considering a quadratic evolution of the transverse displacement with the thickness coordinate.

The governing equations and the boundary conditions are obtained by a generalization of Carrera's Unified Formulation, and further interpolated by collocation with radial basis functions.

Numerical examples on the static analysis of functionally graded sandwich plates demonstrate the accuracy of the present approach. The thickness stretching effect on such problems is studied.

1. Introduction

The strong difference of mechanical properties between faces and core in sandwich structures (or layered composites) introduces a discontinuity of the deformed core-faces planes at the interfaces. This is known as Zig-Zag (ZZ) effect. Such discontinuities make difficult the use of classical theories such as Kirchhoff [1] or Reissner–Mindlin [2,3] type theories (see the books by Zenkert [4], and Vinson [5] to trace accurate responses of sandwich structures). Two possibilities can be used to capture the ZZ effect (see the overviews by Burton and Noor [6], Noor et al. [7], Altenbach [8], Librescu and Hause [9], Vinson [10], and Demasi [11]): the so-called layer-wise models, and a Zig-Zag function (ZZF) in the framework of mixed multilayered plate theories. An historical review on ZZ theories has been provided by Carrera [12].

The first alternative can be computational expensive for laminates with large number of layers as the degrees-of-freedom increase as the number of layers increases. Considering the second alternative, Murakami [13] proposed a ZZF that is able to reproduce the slope discontinuity. Equivalent single layer models with only displacement unknowns can be developed on the basis of ZZF. A review of early developments on the application of ZZF has been provided in the review article by Carrera [14]. The advantages of analyze multilayered anisotropic plate and shells using the ZZF as well as the Finite Element implementation have been discussed by Carrera [15]. Further studies on the use of Murakami's Zig-Zag function (MZZF) have been documented in [15–17].

The use of alternative methods to the Finite Element Methods for the analysis of plates, such as the meshless methods based on radial basis functions (RBFs) is attractive due to the absence of a mesh and the ease of collocation methods. The use of radial basis function for the analysis of structures and materials has been previously studied by numerous authors [18–34].

Carrera's Unified Formulation (CUF) was proposed in [14,35,36] for laminated plates and shells and extended to functionally graded (FG) plates in [37–39]. The present formulation is a generalization of the original CUF in the sense that considers different displacement fields for in-plane and out-of-plane displacements.

In this paper the application of ZZF to bending analysis of thin and thick FG sandwich plates is studied. A new displacement theory is used, considering a quadratic variation of the transverse displacements (allowing for through-the-thickness deformations), and introducing a hyperbolic sine term in the in-plane displacement expansion. This can be seen as a variation of the original Murakami's ZZ displacement field. CUF is combined with RBFs for the static analysis: the principle of virtual displacements is used under CUF to obtain the governing equations and boundary equations and these are interpolated by collocation with RBFs.

The paper is organized as follows. The problem we are dealing with is introduced in Section 2. Then, the state-of-the-art review on the use of Zig-Zag functions and the displacement field of the

* Corresponding author.
E-mail address: ferreira@fe.up.pt (A.J.M. Ferreira).

0965-9978/$ - see front matter
http://dx.doi.org/10.1016/j.advengsoft.2012.05.005

Nomenclature

CUF	Carrera's Unified Formulation
FG	Functionally graded
FGM	Functionally graded material
FSDT	First-order shear deformation theory
MZZF	Murakami's Zig-Zag function
PDE	Partial differential equations
PVD	Principle of virtual displacements
RBF	Radial basis function
SSSS	Simply-supported
ZZ	Zig-Zag
ZZF	Zig-Zag function

present shear deformation theory is presented in Section 3. For the sake of completeness CUF and the radial basis functions collocation technique for the static analysis of FG plates are briefly reviewed in Sections 4 and 5, respectively. Numerical examples on the static analysis of simply supported functionally graded sandwich square plates are presented and discussed in Section 6. These include the computation of the displacements and stresses of sandwich plates with FGM in the core or in the skins, considering several material power-law exponents, side-to-thickness ratios and skin-core-skin ratios as well. Final conclusions are presented in Section 7.

2. Problem formulation

Consider a rectangular plate of plan-form dimensions a and b and uniform thickness h. The co-ordinate system is taken such that the x-y plane ($z = 0$) coincides with the midplane of the plate ($z \in [-h/2, h/2]$). The plate is subjected to a transverse mechanical load applied at the top of the plate.

Two different types of functionally graded sandwich plates are studied: sandwich plates with FG core and sandwich plates with FG skins.

In the sandwich plate with FG core the bottom skin is fully metal (isotropic) and the top skin is fully ceramic (isotropic as well). The core layer is graded from metal to ceramic so that there are no interfaces between core and skins, as illustrated in Fig. 1. The volume fraction of the ceramic phase in the core is obtained by adapting the typical polynomial material law as:

$$V_c = \left(0.5 + \frac{z_c}{h_c}\right)^p \tag{1}$$

where $z_c \in [h_1, h_2]$, $h_c = h_2 - h_1$ is the thickness of the core, and $p > 0$ is the power-law exponent that defines the gradation of material properties across the thickness direction as shown in Fig. 3 (left).

In sandwich plates with FG skins the core is fully ceramic (isotropic) and skins are composed of a functionally graded material across the thickness direction. The bottom skin varies from a metal-rich surface ($z = -h/2$) to a ceramic-rich surface while the top skin face varies from a ceramic-rich surface to a metal-rich surface ($z = h/2$), as illustrated in Fig. 2. There are no interfaces between core and skins. The volume fraction of the ceramic phase in the skins is obtained as:

$$\begin{aligned} V_c &= \left(\tfrac{z-h_0}{h_1-h_0}\right)^p, \quad z \in [-h/2, h_1] \\ V_c &= \left(\tfrac{z-h_3}{h_2-h_3}\right)^p, \quad z \in [h_2, h/2] \end{aligned} \tag{2}$$

where $p \geqslant 0$ is a scalar parameter that allows the user to define gradation of material properties across the thickness direction of the skins. The $p = 0$ case corresponds to the (isotropic) fully ceramic plate.

The sandwich plate with FG skins may be symmetric or non-symmetric about the mid-plane as we may vary the thickness of each face. Fig. 3 (right) shows a non-symmetric sandwich with volume fraction defined by the power-law (2) for various exponents p, in which top skin thickness is the same as the core thickness and the bottom skin thickness is twice the core thickness. Such thickness relation is denoted as 2-1-1. A bottom-core-top notation is

Fig. 1. Sandwich plate with FG core and isotropic skins.

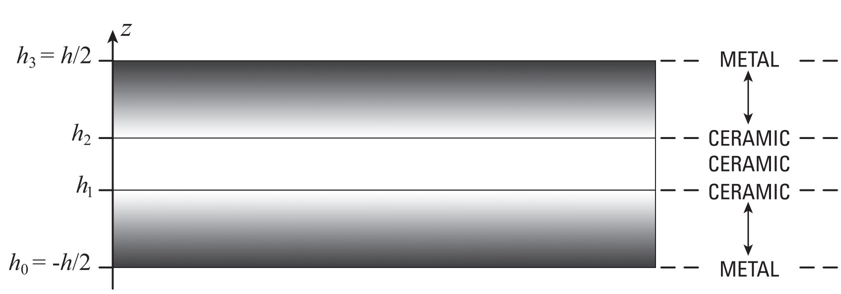

Fig. 2. Sandwich plate with isotropic core and FG skins.

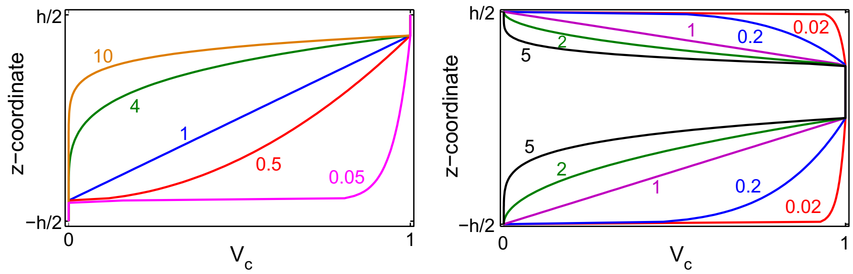

Fig. 3. Effect of the power-law exponent in a sandwich plate with FG core (left) and in a 2-1-1 sandwich plate with FG skins (right).

being used. 1-1-1 means that skins and core have the same thickness.

In both sandwich plates the volume fraction for the metal phase is given as $V_m = 1 - V_c$.

3. A new hyperbolic sine ZZF theory

3.1. The Zig-Zag function

The Murakami's Zig-Zag function $Z(z)$ dependes on the adimensioned layer coordinate, ζ_k, according to the following formula:

$$Z(z) = (-1)^k \zeta_z \tag{3}$$

ζ_k is defined as $\zeta_k = \frac{2z_k}{h_k}$ where z_k is the layer thickness coordinate and h_k is the thickness of the kth layer.

$Z(z)$ has the following properties:

(1) It is a piece-wise linear function of layer coordinates z_k.
(2) $Z(z)$ has unit amplitude for the whole layers.
(3) The slope $Z\prime(z) = \frac{dZ}{dz}$ assumes opposite sign between two-adjacent layers. Its amplitude is layer thickness independent.

3.2. Overview on Murakami's Zig-Zag theories

In 1986, a refinement of FSDT by inclusion of ZZ effects and transverse normal strains was introduced in Murakami's original ZZF [13], defined by the following displacement field:

$$\begin{cases} u = u_0 + zu_1 + (-1)^k \frac{2}{h_k}\left(z - \frac{1}{2}(z_k + z_{k+1})\right)u_Z \\ v = v_0 + zv_1 + (-1)^k \frac{2}{h_k}\left(z - \frac{1}{2}(z_k + z_{k+1})\right)v_Z \\ w = w_0 + zw_1 + (-1)^k \frac{2}{h_k}\left(z - \frac{1}{2}(z_k + z_{k+1})\right)w_Z \end{cases} \tag{4}$$

where u and v are the in-plane displacements and w is the transverse displacement. The involved unknowns are u_0, u_1, u_Z, v_0, v_1, v_Z, w_0, w_1, and w_Z: u_0, v_0 and w_0 are translations of a point at the mid-plane; u_1, v_1 and w_1 are rotations as in the typical FSDT; and the additional degrees of freedom u_Z, v_Z and w_Z have a meaning of displacement. z_k, z_{k+1} are the bottom and top z-coordinates at each layer.

More recently, another possible FSDT theory has been investigated by Carrera [15] and Demasi [16], ignoring the through-the-thickness deformations:

$$\begin{cases} u = u_0 + zu_1 + (-1)^k \frac{2}{h_k}\left(z - \frac{1}{2}(z_k + z_{k+1})\right)u_Z \\ v = v_0 + zv_1 + (-1)^k \frac{2}{h_k}\left(z - \frac{1}{2}(z_k + z_{k+1})\right)v_Z \\ w = w_0 \end{cases} \tag{5}$$

with u_0, u_1, u_Z, v_0, v_1, v_Z, w_0, z_k, and z_{k+1} as before.

Ferreira et al. [40] and Rodrigues et al. [41] used a ZZF theory involving the following expansion of displacements

$$\begin{cases} u = u_0 + zu_1 + (-1)^k \frac{2}{h_k}\left(z - \frac{1}{2}(z_k + z_{k+1})\right)u_Z \\ v = v_0 + zv_1 + (-1)^k \frac{2}{h_k}\left(z - \frac{1}{2}(z_k + z_{k+1})\right)v_Z \\ w = w_0 + zw_1 + z^2 w_2 \end{cases} \tag{6}$$

This represents a variation of the Murakami's original theory, allowing for a quadratic evolution of the transverse displacement across the thickness direction. Furthermore, Ferreira et al. [42] used two higher order ZZF theories allowing for a quadratic evolution of the transverse displacement across the thickness direction as well and involving the following displacement fields:

$$\begin{cases} u = u_0 + zu_1 + z^3 u_3 + (-1)^k \frac{2}{h_k}\left(z - \frac{1}{2}(z_k + z_{k+1})\right)u_Z \\ v = v_0 + zv_1 + z^3 v_3 + (-1)^k \frac{2}{h_k}\left(z - \frac{1}{2}(z_k + z_{k+1})\right)v_Z \\ w = w_0 + zw_1 + z^2 w_2 \end{cases} \tag{7}$$

$$\begin{cases} u = u_0 + zu_1 + sin\left(\frac{\pi z}{h}\right)u_3 + (-1)^k \frac{2}{h_k}\left(z - \frac{1}{2}(z_k + z_{k+1})\right)u_Z \\ v = v_0 + zv_1 + sin\left(\frac{\pi z}{h}\right)v_3 + (-1)^k \frac{2}{h_k}\left(z - \frac{1}{2}(z_k + z_{k+1})\right)v_Z \\ w = w_0 + zw_1 + z^2 w_2 \end{cases} \tag{8}$$

In Eqs. (7) and (8), w_2 denote higher-order translations and u_3 and v_3 denote rotations. u_0, v_0, w_0, u_1, v_1, w_1, u_z, and v_z, are as in (4)–(6).

3.3. The hyperbolic sine ZZF shear deformation theory

All previous cited work using ZZ functions deals with laminated plates or shells. In the present work a new hyperbolic sine ZZF theory is introduced for the analysis of functionally graded sandwich plates. The choice of the new displacement field is based on previous work by the authors and the role of the Zig-Zag effect on sandwich structures. The authors have sucessfuly used a hyperbolic sine quasi-3D shear deformation theory accounting for thickness stretching without the Zig-Zag effect in the study of functionally graded plates [43]. The present theory adds the terms to consider the Zig-Zag effect. The present theory is based on the following displacement field:

$$\begin{cases} u = u_0 + zu_1 + sinh\left(\frac{\pi z}{h}\right)u_3 + (-1)^k \frac{2}{h_k}\left(z - \frac{1}{2}(z_k + z_{k+1})\right)u_Z \\ v = v_0 + zv_1 + sinh\left(\frac{\pi z}{h}\right)v_3 + (-1)^k \frac{2}{h_k}\left(z - \frac{1}{2}(z_k + z_{k+1})\right)v_Z \\ w = w_0 + zw_1 + z^2 w_2 \end{cases} \tag{9}$$

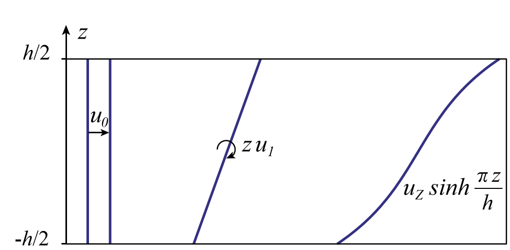

Fig. 4. Scheme of the expansions involved in the displacement field.

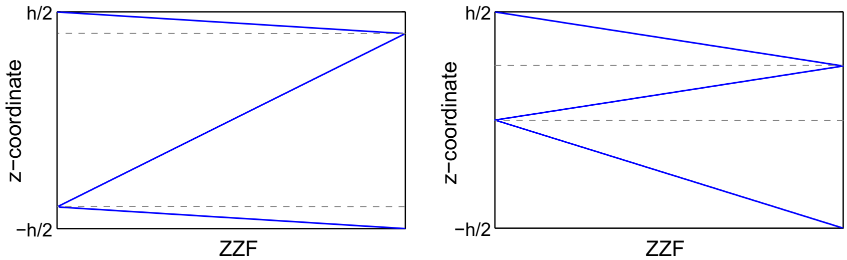

Fig. 5. Zig-Zag effect for the 1-8-1 (left) and the 2-1-1 sandwichs (right).

The involved unknowns have the same meaning as in equations (7) and (8). The expansion of the degrees of freedom u_0, u_1, u_3, v_0, v_1, v_3, w_0, w_1, and w_2 are functions of the thickness coordinate only. These are layer-independent, unlike those of u_Z and v_Z, as illustrated in Figs. 4 and 5. Fig. 4 shows the meaning of the unknows in the in-plane displacements expansion in present theory: u_0, v_0 (translations), u_1, v_1 (rotations), u_3 and v_3 (rotations). In Fig. 5 one can visualize that this ZZF correspondence to a rotation per layer.

4. The Unified Formulation for the static analysis of FG sandwich plates

In this section it is shown how to obtain the fundamental nuclei under CUF, which allows the derivation of the governing equations and boundary conditions for FG plates.

4.1. Functionally graded materials

A conventional FG plate considers a continuous variation of material properties over the thickness direction by mixing two different materials [44]. The material properties of the FG plate are assumed to change continuously throughout the thickness of the plate, according to the volume fraction of the constituent materials. Although one can use CUF for one-layer, isotropic plate, we consider a multi-layered plate. In fact, the sandwiches in study present three physical layers, kp = 1, 2, 3, each containing a different displacement field. Nevertheless, we are dealing with functionally graded materials and becomes mandatory to model the continuos variation of properties across the thickness direction. A considerable number of layers is needed to ensure correct computation of material properties at each thickness position, and for that reason we consider $N_l = 91$ virtual (mathematical) layers of constant thickness. In the following, kp refers to physical layers and $k = 1, \ldots, 91$ refers to virtual layers.

The CUF procedure applied to FG materials starts by evaluating the volume fraction of the two constituents for each layer. Then, a homogenization technique is employed to find the values of the modulus of elasticity, E^k, and Poisson's ratio, ν^k, of each layer.

To describe the volume fractions an exponential function can be used as in [45], or the sigmoid function as proposed in [46]. In the present work a power-law function is used as most researchers do [47–50]. In the typical FG plate the power-law function defines the volume fraction of the ceramic phase as:

$$V_c = \left(0.5 + \frac{z}{h}\right)^p \tag{10}$$

where $z \in [-h/2, h/2]$, h is the thickness of the plate, and p is a scalar parameter that allows the user to define gradation of material properties across the thickness direction. In both sandwich plates, the volume fraction of the ceramic phase of the FG layers are obtained by adapting the typical power-law. Furthermore, we need to compute the volume fraction for each layer. In the sandwich plate with FG core case, (1) becomes:

$$\begin{cases} V_c^k = 0, & \text{in the bottom skin} \\ V_c^k = \left(0.5 + \frac{\tilde{z}_c}{h_c}\right)^p, & \text{in the core} \\ V_c^k = 1, & \text{in the top skin} \end{cases} \tag{11}$$

where $\tilde{z}_c$ is the thickness coordinate of a point of each (virtual) core layer, and h_c and p are as in (1).

Considering (2), for the sandwich plate with FG skins case one has:

$$\begin{cases} V_c^k = \left(\frac{\tilde{z}-h_0}{h_1-h_0}\right)^p, & \text{in the bottom skin} \\ V_c^k = 1, & \text{in the core} \\ V_c^k = \left(\frac{\tilde{z}-h_3}{h_2-h_3}\right)^p, & \text{in the top skin} \end{cases} \tag{12}$$

where $\tilde{z}$ is the thickness coordinate of a point of each (virtual) skin layer.

At this step, a homogenization procedure is used. The one considered in present work is the law-of-mixtures, the same used by the referenced authors, which states that:

$$E^k(z) = E_m V_m + E_c V_c; \quad \nu^k(z) = \nu_m V_m + \nu_c V_c \tag{13}$$

Other homogeneization procedures could be used, for example the Mori–Tanaka one [51,52].

4.2. Modeling of the displacement components

According to the Unified Formulation by Carrera, the three displacement components u_x, $u_y(=v)$ and $u_z(=w)$ and their relative variations are modeled as:

$$\begin{aligned} &(u_x, u_y, u_z) = F_\tau\ (u_{x\tau}, u_{y\tau}, u_{z\tau}) \\ &(\delta u_x, \delta u_y, \delta u_z) = F_s\ (\delta u_{xs}, \delta u_{ys}, \delta u_{zs}) \end{aligned} \tag{14}$$

Resorting to the displacement field in Eq. (9), we choose vectors $F_\tau = \left[1 \quad z \quad \sinh\left(\frac{\pi z}{h}\right) \quad (-1)^{kp} \frac{2}{h_{kp}}\left(z - \frac{1}{2}(z_{kp} + z_{kp+1})\right)\right]$ for in-plane displacements and $F_\tau = [1 \quad z \quad z^2]$ for displacement w. In this case, thickness-stretching is considered. For the thickness effect study, in the case that thickness-stretching is not allowed, the vector for transverse displacement is replaced with $F_\tau = 1$, meaning that we are considering the expansion $w = w_0$ in the displacement field.

4.3. Strains

Strains are separated into in-plane and normal components, denoted respectively by the subscripts p and n. The mechanical strains in the kth layer can be related to the displacement field $\mathbf{u}^k = \left\{u_x^k, u_y^k, u_z^k\right\}$ via the geometrical relations (G):

$$\begin{aligned} &\boldsymbol{\epsilon}_{pG}^k = [\epsilon_{xx}, \epsilon_{yy}, \gamma_{xy}]^{kT} = \mathbf{D}_p^k \mathbf{u}^k, \\ &\boldsymbol{\epsilon}_{nG}^k = [\gamma_{xz}, \gamma_{yz}, \epsilon_{zz}]^{kT} = (\mathbf{D}_{np}^k + \mathbf{D}_{nz}^k)\ \mathbf{u}^k, \end{aligned} \tag{15}$$

wherein the differential operator arrays are defined as follows:

$$\mathbf{D}_p^k = \begin{bmatrix} \partial_x & 0 & 0 \\ 0 & \partial_y & 0 \\ \partial_y & \partial_x & 0 \end{bmatrix}, \quad \mathbf{D}_{np}^k = \begin{bmatrix} 0 & 0 & \partial_x \\ 0 & 0 & \partial_y \\ 0 & 0 & 0 \end{bmatrix}, \quad \mathbf{D}_{nz}^k = \begin{bmatrix} \partial_z & 0 & 0 \\ 0 & \partial_z & 0 \\ 0 & 0 & \partial_z \end{bmatrix}, \tag{16}$$

If $\epsilon_{zz} = 0$ is considered, thickness-stretching is not allowed. In this case, $\boldsymbol{\epsilon}_{pG}^k$ and the differential operator array $\mathbf{D}_p^k$ remain as before, but the other strains are reduced to

$$\boldsymbol{\epsilon}_{nG}^k = [\gamma_{xz}, \gamma_{yz}]^{kT} = \left(\mathbf{D}_{np}^k + \mathbf{D}_{nz}^k\right) \mathbf{u}^k, \tag{17}$$

wherein the differential operator arrays are defined as:

$$\mathbf{D}_{np}^k = \begin{bmatrix} 0 & 0 & \partial_x \\ 0 & 0 & \partial_y \end{bmatrix}, \quad \mathbf{D}_{nz}^k = \begin{bmatrix} \partial_z & 0 & 0 \\ 0 & \partial_z & 0 \end{bmatrix}, \tag{18}$$

4.4. Elastic stress–strain relations

To define the constitutive equations (C), stresses are separated into in-plane and normal components as well.

The 3D constitutive equations are given as:

$$\begin{aligned} \boldsymbol{\sigma}_{pC}^k &= [\sigma_{xx}, \sigma_{yy}, \sigma_{xy}]^{kT} = \mathbf{C}_{pp}^k\ \boldsymbol{\epsilon}_{pG}^k + \mathbf{C}_{pn}^k\ \boldsymbol{\epsilon}_{nG}^k \\ \boldsymbol{\sigma}_{nC}^k &= [\sigma_{xz}, \sigma_{yz}, \sigma_{zz}]^{kT} = \mathbf{C}_{np}^k\ \boldsymbol{\epsilon}_{pG}^k + \mathbf{C}_{nn}^k\ \boldsymbol{\epsilon}_{nG}^k \end{aligned} \tag{19}$$

with

$$\begin{aligned} \mathbf{C}_{pp}^k &= \begin{bmatrix} C_{11}^k & C_{12}^k & 0 \\ C_{12}^k & C_{22}^k & 0 \\ 0 & 0 & C_{66}^k \end{bmatrix} \qquad \mathbf{C}_{pn}^k = \begin{bmatrix} 0 & 0 & C_{13}^k \\ 0 & 0 & C_{23}^k \\ 0 & 0 & 0 \end{bmatrix} \\ \mathbf{C}_{np}^k &= \begin{bmatrix} 0 & 0 & 0 \\ 0 & 0 & 0 \\ C_{13}^k & C_{23}^k & 0 \end{bmatrix} \qquad \mathbf{C}_{nn}^k = \begin{bmatrix} C_{55}^k & 0 & 0 \\ 0 & C_{44}^k & 0 \\ 0 & 0 & C_{33}^k \end{bmatrix} \end{aligned} \tag{20}$$

and the C_{ij}^k are the three-dimensional elastic constants

$$\begin{aligned} C_{11}^k &= C_{22}^k = C_{33}^k = \tfrac{E^k(1-(\nu^k)^2)}{1-3(\nu^k)^2-2(\nu^k)^3}, \\ C_{12}^k &= C_{13}^k = C_{23}^k = \tfrac{E^k(\nu^k+(\nu^k)^2)}{1-3(\nu^k)^2-2(\nu^k)^3}, \\ C_{44}^k &= C_{55}^k = C_{66}^k = G^k \end{aligned} \tag{21}$$

where the modulus of elasticity and Poisson's ratio were defined in (13), and G is the shear modulus $G^k = \frac{E^k}{2(1+\nu^k)}$.

For the $\epsilon_{zz} = 0$ case, the plane-stress case is used:

$$\begin{aligned} \boldsymbol{\sigma}_{pC}^k &= [\sigma_{xx}, \sigma_{yy}, \sigma_{xy}]^{kT} = \mathbf{C}_{pp}^k\ \boldsymbol{\epsilon}_{pG}^k \\ \boldsymbol{\sigma}_{nC}^k &= [\sigma_{xz}, \sigma_{yz}]^{kT} = \mathbf{C}_{nn}^k\ \boldsymbol{\epsilon}_{nG}^k \end{aligned} \tag{22}$$

with $\mathbf{C}_{pp}^k$ and $\boldsymbol{\epsilon}_{pG}^k$ as before, $\boldsymbol{\epsilon}_{nG}^k = [\gamma_{xz}, \gamma_{yz}]^{kT}$ and

$$\mathbf{C}_{nn}^k = \begin{bmatrix} C_{55}^k & 0 \\ 0 & C_{44}^k \end{bmatrix} \tag{23}$$

and C_{ij}^k are the plane-stress reduced elastic constants:

$$C_{11}^k = C_{22}^k = \frac{E^k}{1-(\nu^k)^2}, \quad C_{12}^k = \nu^k \frac{E^k}{1-(\nu^k)^2}, \tag{24}$$

$$C_{44}^k = C_{55}^k = C_{66}^k = G^k \tag{25}$$

4.5. Principle of virtual displacements

In the framework of the Unified Formulation, the Principle of Virtual Displacements (PVD) for the pure-mechanical case is written as:

$$\sum_{k=1}^{N_l} \int_{\Omega_k} \int_{A_k} \left\{ \delta\boldsymbol{\epsilon}_{pG}^{k\ T} \boldsymbol{\sigma}_{pC}^k + \delta\boldsymbol{\epsilon}_{nG}^{k\ T} \boldsymbol{\sigma}_{nC}^k \right\} d\Omega_k dz = \sum_{k=1}^{N_l} \delta L_e^k \tag{26}$$

where Ω_k and A_k are the integration domains in plane (x,y) and z direction, respectively. As stated before, G means geometrical relations and C constitutive equations, and k indicates the virtual layer. T is the transpose operator and δL_e^k is the external work for the kth layer.

Substituting the geometrical relations (G), the constitutive equations (C), and the modeled displacement field (F_τ and F_s), all for the kth layer, (26) becomes:

$$\begin{aligned} &\int_{\Omega_k} \int_{A_k} \Bigg[\left(\mathbf{D}_p^k F_s \delta\mathbf{u}_s^k\right)^T \left(\mathbf{C}_{pp}^k \mathbf{D}_p^k F_\tau \mathbf{u}_\tau^k + \mathbf{C}_{pn}^k (\mathbf{D}_{n\Omega}^k + \mathbf{D}_{nz}^k) F_\tau \mathbf{u}_\tau^k\right) \\ &\quad + \left(\left(\mathbf{D}_{n\Omega}^k + \mathbf{D}_{nz}^k\right) F_s \delta\mathbf{u}_s^k\right)^T \left(\mathbf{C}_{np}^k \mathbf{D}_p^k F_\tau \mathbf{u}_\tau^k + \mathbf{C}_{nn}^k (\mathbf{D}_{n\Omega}^k + \mathbf{D}_{nz}^k) F_\tau \mathbf{u}_\tau^k\right) \Bigg] d\Omega_k dz \\ &= \delta L_e^k \end{aligned} \tag{27}$$

Applying now the formula of integration by parts, (27) becomes:

$$\begin{aligned} \int_{\Omega_k} ((\mathbf{D}_\Omega)\delta\mathbf{a}^k)^T \mathbf{a}^k d\Omega_k &= -\int_{\Omega_k} \delta\mathbf{a}^{kT} \left(\left(\mathbf{D}_\Omega^T\right)\mathbf{a}^k\right) d\Omega_k \\ &\quad + \int_{\Gamma_k} \delta\mathbf{a}^{kT} ((\mathbf{I}_\Omega)\mathbf{a}^k) d\Gamma_k \end{aligned} \tag{28}$$

where $\mathbf{I}_\Omega$ matrix is obtained applying the *Gradient theorem*:

$$\int_\Omega \frac{\partial\psi}{\partial x_i} d\upsilon = \oint_\Gamma n_i \psi ds \tag{29}$$

being n_i the components of the normal $\hat{n}$ to the boundary along the direction i. After integration by parts, the governing equations and boundary conditions for the plate in the mechanical case are obtained:

$$\begin{aligned} &\int_{\Omega_k} \int_{A_k} (\delta\mathbf{u}_s^k)^T \Bigg[\Bigg(\left(-\mathbf{D}_p^k\right)^T \left(\mathbf{C}_{pp}^k (\mathbf{D}_p^k) + \mathbf{C}_{pn}^k (\mathbf{D}_{n\Omega}^k) + \mathbf{D}_{nz}^k\right) \\ &\quad + \left(-\mathbf{D}_{n\Omega}^k + \mathbf{D}_{nz}^k\right)^T \left(\mathbf{C}_{np}^k (\mathbf{D}_p^k) + \mathbf{C}_{nn}^k (\mathbf{D}_{n\Omega}^k + \mathbf{D}_{nz}^k)\right) \Bigg) \mathbf{F}_\tau \mathbf{F}_s \mathbf{u}_\tau^k \Bigg] dxdydz \\ &\quad + \int_{\Omega_k} \int_{A_k} (\delta\mathbf{u}_s^k)^T \Bigg[\Bigg(\mathbf{I}_p^{kT} \left(\mathbf{C}_{pp}^k (\mathbf{D}_p^k)\ + \mathbf{C}_{pn}^k (\mathbf{D}_{n\Omega}^k + \mathbf{D}_{nz}^k)\right) + \mathbf{I}_{np}^{kT} \Big(\mathbf{C}_{np}^k \left(\mathbf{D}_p^k\right) \\ &\quad + \mathbf{C}_{nn}^k \left(\mathbf{D}_{n\Omega}^k + \mathbf{D}_{nz}^k\right)\Big)\Bigg) \mathbf{F}_\tau \mathbf{F}_s \mathbf{u}_\tau^k \Bigg] dxdydz = \int_{\Omega_k} \delta\mathbf{u}_s^{kT} F_s \mathbf{p}_u^k d\Omega_k. \end{aligned} \tag{30}$$

where $\mathbf{I}_p^k$ and $\mathbf{I}_{np}^k$ depend on the boundary geometry:

$$\mathbf{I}_p^k = \begin{bmatrix} n_x & 0 & 0 \\ 0 & n_y & 0 \\ n_y & n_x & 0 \end{bmatrix}, \quad \mathbf{I}_{np}^k = \begin{bmatrix} 0 & 0 & n_x \\ 0 & 0 & n_y \\ 0 & 0 & 0 \end{bmatrix}. \tag{31}$$

The normal to the boundary of domain Ω is:

$$\hat{\mathbf{n}} = \begin{bmatrix} n_x \\ n_y \end{bmatrix} = \begin{bmatrix} cos(\varphi_x) \\ cos(\varphi_y) \end{bmatrix} \tag{32}$$

where φ_x and φ_y are the angles between the normal $\hat{n}$ and the direction x and y respectively.

4.6. Governing equations and boundary conditions

The governing equations for a multi-layered plate subjected to mechanical loadings are:

$$\delta\mathbf{u}_s^{k^T} : \mathbf{K}_{uu}^{k\tau s}\ \mathbf{u}_\tau^k = \mathbf{P}_{u\tau}^k \tag{33}$$

where the fundamental nucleus $\mathbf{K}_{uu}^{k\tau s}$ is obtained as:

$$
\begin{aligned}
\mathbf{K}_{uu}^{k\tau s} = \Big[& \left(-\mathbf{D}_p^k\right)^T \left(\mathbf{C}_{pp}^k \left(\mathbf{D}_p^k\right) + \mathbf{C}_{pn}^k (\mathbf{D}_{n\Omega}^k) + \mathbf{D}_{nz}^k\right) \\
& + \left(-\mathbf{D}_{n\Omega}^k + \mathbf{D}_{nz}^k\right)^T \left(\mathbf{C}_{np}^k (\mathbf{D}_p^k) + \mathbf{C}_{nn}^k (\mathbf{D}_{n\Omega}^k + \mathbf{D}_{nz}^k)\right)\Big] \mathbf{F}_\tau \mathbf{F}_s
\end{aligned} \tag{34}
$$

and the corresponding Neumann-type boundary conditions on Γ_k are:

$$
\mathbf{\Pi}_d^{k\tau s}\ \mathbf{u}_\tau^k = \mathbf{\Pi}_d^{k\tau s}\ \bar{\mathbf{u}}_\tau^k, \tag{35}
$$

where:

$$
\begin{aligned}
\mathbf{\Pi}_d^{k\tau s} = \Big[& \mathbf{I}_p^{kT} \left(\mathbf{C}_{pp}^k \left(\mathbf{D}_p^k\right) + \mathbf{C}_{pn}^k (\mathbf{D}_{n\Omega}^k + \mathbf{D}_{nz}^k)\right) \\
& + \mathbf{I}_{np}^{kT} \left(\mathbf{C}_{np}^k (\mathbf{D}_p^k) + \mathbf{C}_{nn}^k (\mathbf{D}_{n\Omega}^k + \mathbf{D}_{nz}^k)\right)\Big] \mathbf{F}_\tau \mathbf{F}_s
\end{aligned} \tag{36}
$$

and $\mathbf{P}_{u\tau}^k$ are variationally consistent loads with applied pressure.

For FG materials, the fundamental nuclei in explicit form becomes:

$$
\begin{aligned}
K_{uu_{11}}^{k\tau s} &= \left(-\partial_x^\tau \partial_x^s C_{11} + \partial_z^\tau \partial_z^s C_{55} - \partial_y^\tau \partial_y^s C_{66}\right) F_\tau F_s \\
K_{uu_{12}}^{k\tau s} &= \left(-\partial_x^\tau \partial_y^s C_{12} - \partial_y^\tau \partial_x^s C_{66}\right) F_\tau F_s \\
K_{uu_{13}}^{k\tau s} &= (-\partial_x^\tau \partial_z^s C_{13} + \partial_z^\tau \partial_x^s C_{55}) F_\tau F_s \\
K_{uu_{21}}^{k\tau s} &= \left(-\partial_y^\tau \partial_x^s C_{12} - \partial_x^\tau \partial_y^s C_{66}\right) F_\tau F_s \\
K_{uu_{22}}^{k\tau s} &= \left(-\partial_y^\tau \partial_y^s C_{22} + \partial_z^\tau \partial_z^s C_{44} - \partial_x^\tau \partial_x^s C_{66}\right) F_\tau F_s \\
K_{uu_{23}}^{k\tau s} &= \left(-\partial_y^\tau \partial_z^s C_{23} + \partial_z^\tau \partial_y^s C_{44}\right) F_\tau F_s \\
K_{uu_{31}}^{k\tau s} &= (\partial_z^\tau \partial_x^s C_{13} - \partial_x^\tau \partial_z^s C_{55}) F_\tau F_s \\
K_{uu_{32}}^{k\tau s} &= \left(\partial_z^\tau \partial_y^s C_{23} - \partial_y^\tau \partial_z^s C_{44}\right) F_\tau F_s \\
K_{uu_{33}}^{k\tau s} &= \left(\partial_z^\tau \partial_z^s C_{33} - \partial_y^\tau \partial_y^s C_{44} - \partial_x^\tau \partial_x^s C_{55}\right) F_\tau F_s
\end{aligned} \tag{37}
$$

$$
\begin{aligned}
\Pi_{11}^{k\tau s} &= \left(n_x \partial_x^s C_{11} + n_y \partial_y^s C_{66}\right) F_\tau F_s \\
\Pi_{12}^{k\tau s} &= \left(n_x \partial_y^s C_{12} + n_y \partial_x^s C_{66}\right) F_\tau F_s \\
\Pi_{13}^{k\tau s} &= (n_x \partial_z^s C_{13}) F_\tau F_s \\
\Pi_{21}^{k\tau s} &= \left(n_y \partial_x^s C_{12} + n_x \partial_y^s C_{66}\right) F_\tau F_s \\
\Pi_{22}^{k\tau s} &= \left(n_y \partial_y^s C_{22} + n_x \partial_x^s C_{66}\right) F_\tau F_s \\
\Pi_{23}^{k\tau s} &= (n_y \partial_z^s C_{23}) F_\tau F_s \\
\Pi_{31}^{k\tau s} &= (n_x \partial_z^s C_{55}) F_\tau F_s \\
\Pi_{32}^{k\tau s} &= (n_y \partial_z^s C_{44}) F_\tau F_s \\
\Pi_{33}^{k\tau s} &= \left(n_y \partial_y^s C_{44} + n_x \partial_x^s C_{55}\right) F_\tau F_s
\end{aligned} \tag{38}
$$

5. The radial basis function method applied to static problems

Recently, radial basis functions (RBFs) have enjoyed considerable success and research as a technique for interpolating data and functions. A radial basis function, $\phi(\|x - x_j\|)$ is a spline that depends on the Euclidian distance between distinct data centers $x_j,\ j = 1, 2, \ldots, N \in \mathbb{R}^n$, also called nodal or collocation points. Although most work to date on RBFs relates to scattered data approximation and in general to interpolation theory, there has recently been an increased interest in their use for solving partial differential equations (PDEs). This approach, which approximates the whole solution of the PDE directly using RBFs, is truly a mesh-free technique. Kansa [53] introduced the concept of solving PDEs by an unsymmetric RBF collocation method based upon the MQ interpolation functions, in which the shape parameter may vary across the problem domain.

The radial basis function (ϕ) approximation of a function ($\mathbf{u}$) is given by

$$
\tilde{\mathbf{u}}(\mathbf{x}) = \sum_{i=1}^{N} \alpha_i \phi(\|x - y_i\|_2), \mathbf{x} \in \mathbb{R}^n \tag{39}
$$

where y_i, $i = 1, \ldots, N$ is a finite set of distinct points (centers) in $\mathbb{R}^n$.

The most common RBFs are

$$
\begin{aligned}
&\text{Cubic}: \quad \phi(r) = r^3 \\
&\text{Thin plate splines}: \quad \phi(r) = r^2 \log(r) \\
&\text{Wendland functions}: \quad \phi(r) = (1 - r)_+^m p(r) \\
&\text{Gaussian}: \quad \phi(r) = e^{-(cr)^2} \\
&\text{Multiquadrics}: \quad \phi(r) = \sqrt{c^2 + r^2} \\
&\text{Inverse Multiquadrics}: \quad \phi(r) = (c^2 + r^2)^{-1/2}
\end{aligned}
$$

where the Euclidian distance r is real and non-negative and c is a positive shape parameter. In the present work, we consider the compact-support Wendland function defined as

$$
\phi(r) = (1 - c\ r)_+^8 (32(c\ r)^3 + 25(c\ r)^2 + 8c\ r + 1) \tag{40}
$$

The shape parameter (c) is obtained by an optimization procedure, as detailed in Ferreira and Fasshauer [54].

Considering N distinct interpolations, and knowing $u(x_j)$, $j = 1, 2, \ldots, N$, we find α_i by the solution of a $N \times N$ linear system

$$
\mathbf{A}\boldsymbol{\alpha} = \mathbf{u} \tag{41}
$$

where $\mathbf{A} = [\phi(\|x - y_i\|_2)]_{N \times N}$, $\boldsymbol{\alpha} = [\alpha_1, \alpha_2, \ldots, \alpha_N]^T$ and $\mathbf{u} = [u(x_1), u(x_2), \ldots, u(x_N)]^T$.

Consider a linear elliptic partial differential operator $\mathcal{L}$ acting in a bounded region Ω in $\mathbb{R}^n$ and another operator $\mathcal{L}_B$ acting on a boundary $\partial\Omega$. In the static problems we seek the computation of displacements ($\mathbf{u}$) from the global system of equations

$$
\mathcal{L}\mathbf{u} = \mathbf{f} \text{ in } \Omega \tag{42}
$$

$$
\mathcal{L}_B\mathbf{u} = \mathbf{g} \text{ on } \partial\Omega \tag{43}
$$

The right-hand side of (42) and (43) represent the external forces applied on the plate and the boundary conditions applied along the perimeter of the plate, respectively. The PDE problem defined in (42) and (43) will be replaced by a finite problem, defined by an algebraic system of equations, after the radial basis expansions.

The solution of a static problem by radial basis functions considers N_I nodes in the domain and N_B nodes on the boundary, with a total number of nodes $N = N_I + N_B$. In the present work, a $\Re^2$ Chebyshev grid is employed (see Fig. 6) and a square plate is com-

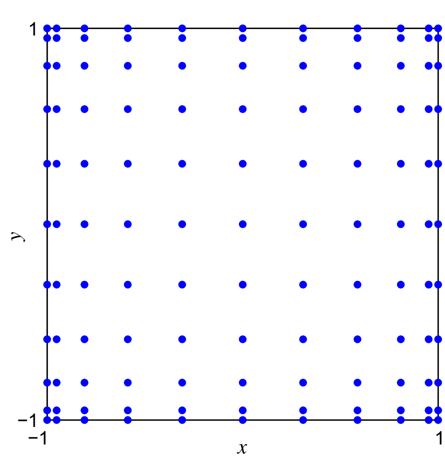

Fig. 6. A sketch of a $\Re^2$ Chebyshev grid with 11^2 points.

puted with side length $a = 2$. For a given number of nodes per side $(N+1)$ they are generated by MATLAB code as:

```
x = cos(pi*(0:N)/N)'; y = x;
```

One advantage of such mesh is the concentration of points near the boundary.

We denote the sampling points by $x_i \in \Omega$, $i = 1, \ldots, N_I$ and $x_i \in \partial\Omega$, $i = N_I + 1, \ldots, N$. At the points in the domain we solve the following system of equations

$$\sum_{i=1}^{N} \alpha_i \mathcal{L}\phi(\|x - y_i\|_2) = \mathbf{f}(x_j), \quad j = 1, 2, \ldots, N_I \tag{44}$$

or

$$\mathcal{L}^I \boldsymbol{\alpha} = \mathbf{F} \tag{45}$$

where

$$\mathcal{L}^I = [\mathcal{L}\phi(\|x - y_i\|_2)]_{N_I \times N} \tag{46}$$

At the points on the boundary, we impose boundary conditions as

$$\sum_{i=1}^{N} \alpha_i \mathcal{L}_B \phi(\|x - y_i\|_2) = \mathbf{g}(x_j), \quad j = N_I + 1, \ldots, N \tag{47}$$

or

$$\mathbf{B}\boldsymbol{\alpha} = \mathbf{G} \tag{48}$$

where

$$\mathbf{B} = \mathcal{L}_B \phi[(\|x_{N_I+1} - y_j\|_2)]_{N_B \times N}$$

Therefore, we can write a finite-dimensional static problem as

$$\begin{bmatrix} \mathcal{L}^I \\ \mathbf{B} \end{bmatrix} \boldsymbol{\alpha} = \begin{bmatrix} \mathbf{F} \\ \mathbf{G} \end{bmatrix} \tag{49}$$

By inverting the system (49), we obtain the vector $\boldsymbol{\alpha}$. We then obtain the solution $\mathbf{u}$ using the interpolation Eq. (39).

The radial basis collocation method follows a simple implementation procedure. Taking Eq. (49), we compute

$$\boldsymbol{\alpha} = \begin{bmatrix} L^I \\ \mathbf{B} \end{bmatrix}^{-1} \begin{bmatrix} \mathbf{F} \\ \mathbf{G} \end{bmatrix} \tag{50}$$

This $\boldsymbol{\alpha}$ vector is then used to obtain solution $\tilde{\mathbf{u}}$, by using (39). If derivatives of $\tilde{\mathbf{u}}$ are needed, such derivatives are computed as

$$\frac{\partial \tilde{\mathbf{u}}}{\partial x} = \sum_{j=1}^{N} \alpha_j \frac{\partial \phi_j}{\partial x} \tag{51}$$

$$\frac{\partial^2 \tilde{\mathbf{u}}}{\partial x^2} = \sum_{j=1}^{N} \alpha_j \frac{\partial^2 \phi_j}{\partial x^2}, \quad \text{etc} \tag{52}$$

In the present collocation approach, we need to impose essential and natural boundary conditions. Consider, for example, the condition $w = 0$, on a simply supported or clamped edge. We enforce the conditions by interpolating as

$$w = 0 \rightarrow \sum_{j=1}^{N} \alpha_j^W \phi_j = 0 \tag{53}$$

Other boundary conditions are interpolated in a similar way.

6. Numerical examples

In this section the shear deformation plate theory is combined with radial basis functions collocation for the static analysis of functionally graded sandwich plates. Displacements and stresses of simply supported (SSSS) square ($a = b = 2$) sandwich plates with FGM in the core or in the skins, both symmetric and unsymmetric, are analyzed. Various side-to-thickness ratios, power-law exponents, and skin-core-skin thickness ratios are considered. The plate is subjected to a bi-sinusoidal transverse mechanical load, $p = p_z \cos\left(\frac{\pi x}{a}\right) \cos\left(\frac{\pi y}{a}\right)$ (see Fig. 6), applied at the top of the plate.

As stated before, all numerical examples are performed employing a Chebyshev grid and the Wendland function as defined in (40) with an optimized shape parameter. The plate is a sandwich, physicaly divided into 3 layers, but we consider 91 virtual layers. The power-law function is used to describe the volume fraction of the metal and ceramic phases (see (1) and (2)) and the material homogeneization technique adopted is the law of mixtures (13), the same used in the references.

The following material properties are used:

$$\text{zirconia Young's modulus}: E_c = 151\ \text{GPa} \tag{54}$$

$$\text{aluminum Young's modulus}: E_m = 70\ \text{GPa} \tag{55}$$

$$\text{alumina Young's modulus}: E_c = 380\ \text{GPa} \tag{56}$$

with Poisson's ratio constant $\nu = 0.3$. Only Young's modulus needs a homogeneization technique.

An initial study was performed for each type of sandwich to show the convergence of the present approach and select the number of Chebyshev points to use in the computation of the static problems problems.

6.1. Sandwich with FG core

The static analysis of sandwich plates with FG core is now performed. In the following examples the materials are aluminum (55) and alumina (56). The thickness of each skin layer is $h_s = 0.1h$ and the core layer thickness is $h_c = 0.8h$, i.e., we are dealing with a 1-8-1 sandwich.

The non-dimensional parameters used are:

$$\begin{aligned}
\bar{w} &= \frac{10E_c h^3}{a^4 p_z} w, \quad \text{evaluated at the center of the plate} \\
\bar{\sigma}_{xx} &= \frac{h}{ap_z}\sigma_{xx}, \quad \text{evaluated at the center of the plate} \\
\bar{\sigma}_{xy} &= \frac{h}{ap_z}\sigma_{xy}, \quad \text{evaluated at the corner of the plate} \\
\bar{\sigma}_{xz} &= \frac{h}{ap_z}\sigma_{xz}, \quad \text{evaluated at the midpoint of the side} \\
\sigma_{zz} &= \sigma_{zz}, \quad \text{evaluated at center of the plate}
\end{aligned} \tag{57}$$

Two convergence studies were performed, varying the exponent power-law p and the side-to-thickness ratio a/h. Table 1 refers to $p = 1$ and $a/h = 4$ and Table 2 refers to $p = 10$ and $a/h = 100$. A 15^2 grid was chosen for the following static problems.

Table 3 and Figs. 7 and 8 refer to the out-of-plane displacement. In Table 3 we tabulate the values of the deflection obtained with

Table 1
Convergence study for a sandwich with FG core with $p = 1$ and $a/h = 4$.

Grid	9^2	11^2	13^2	15^2	17^2	19^2
$\bar{w}(0)$	0.7411	0.7417	0.7417	0.7417	0.7417	0.7417
$\bar{\sigma}_{xx}(\frac{h}{3})$	0.6224	0.6236	0.6235	0.6236	0.6236	0.6236
$\bar{\sigma}_{xy}(\frac{h}{3})$	0.3263	0.3164	0.3164	0.3165	0.3164	0.3164
$\bar{\sigma}_{xz}(0)$	0.2329	0.2333	0.2332	0.2332	0.2332	0.2332
$\bar{\sigma}_{xz}(\frac{h}{6})$	0.2745	0.2748	0.2747	0.2747	0.2747	0.2747
$\bar{\sigma}_{xz}(\frac{h}{3})$	0.2195	0.2193	0.2192	0.2192	0.2192	0.2192
$\sigma_{zz}(0)$	0.3316	0.3311	0.3312	0.3312	0.3312	0.3312

Table 2
Convergence study for a sandwich with FG core with $p = 10$ and $a/h = 100$.

Grid	9^2	11^2	13^2	15^2	17^2	19^2
$\bar{w}(0)$	0.6794	0.8035	0.8009	0.8045	0.8048	0.8050
$\bar{\sigma}_{xx}(\frac{h}{3})$	7.5645	9.1864	9.3955	9.4300	9.4187	9.4272
$\bar{\sigma}_{xy}(\frac{h}{3})$	3.4217	4.9099	5.0405	5.0641	5.0641	5.0735
$\bar{\sigma}_{xz}(0)$	0.2002	0.2188	0.2017	0.2056	0.2047	0.2052
$\bar{\sigma}_{xz}(\frac{h}{6})$	0.1970	0.2216	0.2025	0.2065	0.2055	0.2060
$\bar{\sigma}_{xz}(\frac{h}{3})$	0.2137	0.3072	0.2612	0.2685	0.2657	0.2659
$\sigma_{zz}(0)$	0.2003	0.1858	0.1850	0.1834	0.1850	0.1839

Table 3
$\bar{w}(0)$ of a sandwich plate with FG core, for several exponents p and ratios a/h.

	ϵ_{zz}	$p = 1$	$p = 4$	$p = 5$	$p = 10$
$a/h = 4$					
Ref. LD4 [38]	0	0.7629		1.1327	1.2232
Ref. LM4 [38]	≠0	0.7629		1.1329	1.2244
Ref. [55] $N = 4$	0	0.7735	1.0977		1.2240
Ref. [55] $N = 4$	≠0	0.7628	1.0930		1.2172
Ref. [?]	0	0.7744	1.0847		1.2212
Ref. [?]	≠0	0.7416	1.0391		1.1780
Present	0	0.7746	1.0833	1.1236	1.2183
Present	≠0	0.7417	1.0378	1.0783	1.1753
$a/h = 10$					
Ref. [55] $N = 4$	0	0.6337	0.8308		0.8743
Ref. [55] $N = 4$	≠0	0.6324	0.8307		0.8740
Ref. [?]	0	0.6356	0.8276		0.8718
Ref. [?]	≠0	0.6305	0.8202		0.8650
Present	0	0.6357	0.8273	0.8415	0.8712
Present	≠0	0.6305	0.8200	0.8342	0.8645
$a/h = 100$					
Ref. LD4 [38]	0	0.6073		0.7892	0.8077
Ref. LM4 [38]	≠0	0.6073		0.7892	0.8077
Ref. [55] $N = 4$	0	0.6072	0.7797		0.8077
Ref. [55] $N = 4$	≠0	0.6072	0.7797		0.8077
Ref. [?]	0	0.6092	0.7785		0.8050
Ref. [?]	≠0	0.6092	0.7784		0.8050
Present	0	0.6087	0.7779	0.7870	0.8045
Present	≠0	0.6086	0.7778	0.7870	0.8045

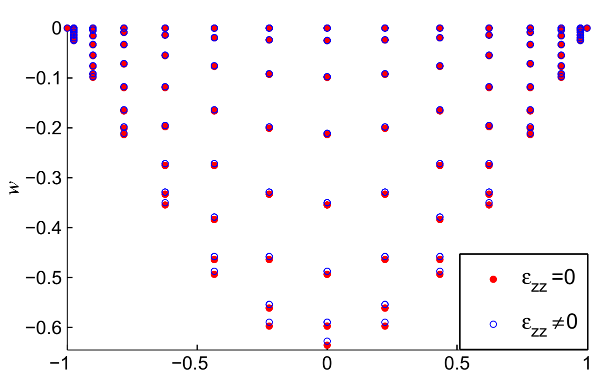

Fig. 7. Deformed of the SSSS sandwich square plate with FG core ($p = 1$, $a/h = 10$), subjected to sinusoidal load at the top, according to the hyperbolic sine ZZ theory, considering and disregarding thickness-stretching.

present approach for various power-law exponents p and side-to-thickness ratios a/h, and compare with available references. In Fig. 7, the thickness-stretching effect on the deformed of the simply supported sandwich square plate with FG core, with $p = 1$ and $a/h = 10$, is visualized. Figure is the plot of the top ($z = h/2$) of the plate. Fig. 8 presents the out-of-plane displacement through

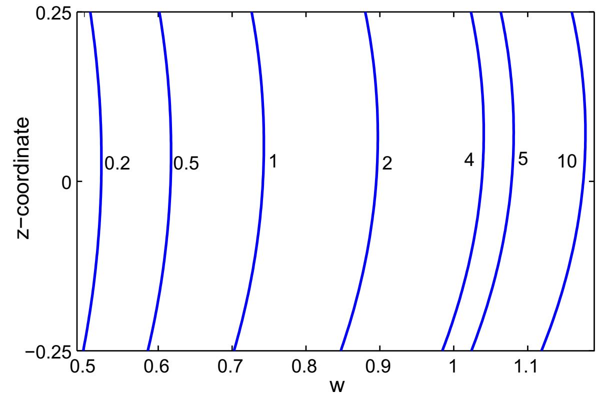

Fig. 8. Out-of-plane displacement through the thickness direction of a SSSS sandwich square plate with FG core, $a/h = 4$, subjected to sinusoidal load at the top, according to the hyperbolic sine ZZ theory, for several values of p.

the thickness direction, for a sandwich with FG core with side-to-thickness ratio $a/h = 4$, varying the exponent power-law value p.

Table 3 and Fig. 8 lead us to the conclusion that the deflection of a SSSS sandwich plate with FG core increases as the power-law exponent of the material p increases. The results depend on consider or neglect warping in the thickness direction. The warping effect is more significative in thicker plates.

Tables 4–8 and Figs. 9–14, refer to stresses. In tables we tabulate and compare with available references the results obtained

Table 4
$\bar{\sigma}_{xx}(h/3)$ of a sandwich plate with FG core, for several exponents p and ratios a/h.

	ϵ_{zz}	$p = 1$	$p = 4$	$p = 5$	$p = 10$
$a/h = 4$					
Ref. LD4 [38]	0	0.6530		0.4693	0.3627
Ref. LM4 [38]	≠0	0.6531		0.4672	0.3611
Present	0	0.6130	0.4643	0.4304	0.3247
Present	≠0	0.6236	0.4605	0.4243	0.3156
$a/h = 10$					
Present	0	1.5700	1.2514	1.1777	0.9214
Present	≠0	1.5743	1.2498	1.1751	0.9176
$a/h = 100$					
Ref. LD4 [38]	0	15.784		12.065	9.5501
Ref. LM4 [38]	≠0	15.784		12.065	9.5500
Present	0	15.7826	12.6971	11.9800	9.4300
Present	≠0	15.7841	12.6975	11.9805	9.4300

Table 5
$\bar{\sigma}_{xy}(h/3)$ of a sandwich plate with FG core, for several exponents p and ratios a/h.

	ϵ_{zz}	$p = 1$	$p = 4$	$p = 5$	$p = 10$
$a/h = 4$					
Ref. LD4 [38]	0	0.3007		0.1999	0.1412
Ref. LM4 [38]	≠0	0.3007		0.1996	0.1403
Ref. [?]	0	0.3303		0.2317	0.1745
Ref. [?]	≠0	0.3167		0.2248	0.1687
Present	0	0.3301	0.2500	0.2318	0.1749
Present	≠0	0.3165	0.2425	0.2249	0.1692
$a/h = 10$					
Present	0	0.8453	0.6738	0.6341	0.4962
Present	≠0	0.8400	0.6709	0.6315	0.4939
$a/h = 100$					
Ref. LD4 [38]	0	8.4968		6.4942	5.1402
Ref. LM4 [38]	≠0	8.4968		6.4942	5.1401
Ref. [?]	0	8.4888		6.4454	5.0745
Ref. [?]	≠0	8.4911		6.4441	5.0754
Present	0	8.4644	6.8194	6.4400	5.0672
Present	≠0	8.4689	6.8102	6.4392	5.0628

Table 6
$\bar{\sigma}_{xz}(0)$ of a sandwich plate with FG core, for several exponents p and ratios a/h.

	ϵ_{zz}	$p = 1$	$p = 4$	$p = 5$	$p = 10$
$a/h = 4$					
Ref. LD4 [38]	0	0.2345		0.1998	0.2113
Ref. LM4 [38]	≠0	0.2345		0.2026	0.2124
Present	0	0.2334	0.1880	0.1863	0.2017
Present	≠0	0.2332	0.1873	0.1857	0.2015
$a/h = 10$					
Present	0	0.2353	0.1905	0.1889	0.2044
Present	≠0	0.2353	0.1900	0.1887	0.2050
$a/h = 100$					
Ref. LD4 [38]	0	0.2375		0.2046	0.2149
Ref. LM4 [38]	≠0	0.2375		0.2055	0.2122
Present	0	0.2367	0.1911	0.1895	0.2050
Present	≠0	0.2368	0.1907	0.1894	0.2056

Table 7
$\bar{\sigma}_{zz}(0) = \frac{h}{ap_z}\sigma_{zz}(\frac{a}{2}, \frac{a}{2}, 0)$ of a sandwich plate with FG core, for several exponents p and ratios a/h.

	ϵ_{zz}	$p = 1$	$p = 4$	$p = 5$	$p = 10$
$a/h = 4$					
Ref. LD4 [38]	0	0.0922		0.0911	0.1064
Ref. LM4 [38]	≠0	0.0922		0.0924	0.1067
Ref. [?]	≠0	0.0827		0.0522	0.0443
Present	≠0	0.0828	0.0580	0.0524	0.0445
$a/h = 10$					
Present	≠0	0.0338	0.0239	0.0216	0.0183
$a/h = 100$					
Ref. LD4 [38]	0	0.0038		0.0037	0.0043
Ref. LM4 [38]	≠0	0.0038		0.0037	0.0042
Ref. [?]	≠0	0.0034		0.0022	0.0018
Present	≠0	0.0034	0.0024	0.0022	0.0018

Table 8
$\bar{\sigma}_{xz}(h/6)$ of a sandwich plate with FG core, for several exponents p and ratios a/h.

	ϵ_{zz}	$p = 1$	$p = 4$	$p = 5$	$p = 10$
$a/h = 4$					
Ref. [55] $N = 4$	0	0.2604	0.2400		0.1932
Ref. [55] $N = 4$	≠0	0.2596	0.2400		0.1935
Ref. [?]	0	0.2703	0.2699		0.1998
Ref. [?]	≠0	0.2742	0.2723		0.2016
Present	0	0.2709	0.2706	0.2537	0.1995
Present	≠0	0.2747	0.2732	0.2560	0.2013
$a/h = 10$					
Ref. [55] $N = 4$	0	0.2594	0.2398		0.1944
Ref. [55] $N = 4$	≠0	0.2593	0.2398		0.1944
Ref. [?]	0	0.2718	0.2726		0.2021
Ref. [?]	≠0	0.2788	0.2778		0.2059
Present	0	0.2724	0.2735	0.2566	0.2017
Present	≠0	0.2793	0.2789	0.2615	0.2055
$a/h = 100$					
Ref. [55] $N = 4$	0	0.2593	0.2398		0.1946
Ref. [55] $N = 4$	≠0	0.2593	0.2398		0.1946
Ref. [?]	0	0.2720	0.2728		0.2022
Ref. [?]	≠0	0.2793	0.2785		0.2064
Present	0	0.2743	0.2747	0.2576	0.2230
Present	≠0	0.2816	0.2805	0.2630	0.2065

with present approach for various exponents of the power-law p and side-to-thickness ratios a/h. In figures we present stresses through the thickness direction of a SSSS sandwich square plate with FG core, $a/h = 100$ according to the hyperbolic sine ZZ theory, for several values of p.

In all tables, results obtained with present hyperbolic sine ZZ theory and RBF collocation are in good agreement with references.

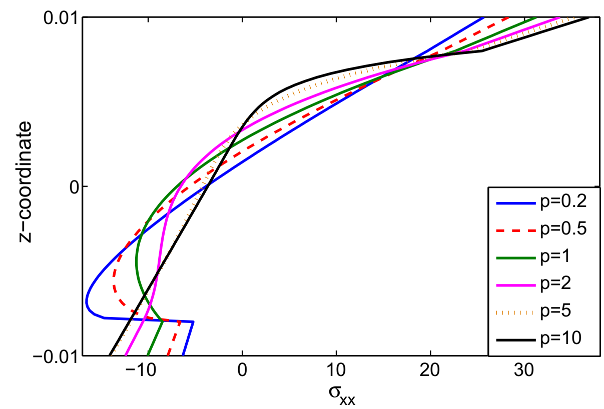

Fig. 9. $\bar{\sigma}_{xx}$ through the thickness direction of a SSSS sandwich square plate with FG core, $a/h = 100$, subjected to sinusoidal load at the top, according to the hyperbolic sine ZZ theory, for several values of p.

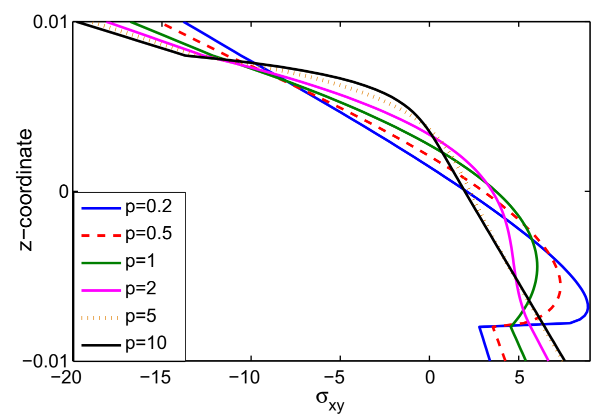

Fig. 10. $\bar{\sigma}_{xy}$ through the thickness direction of a SSSS sandwich square plate with FG core, $a/h = 100$, subjected to sinusoidal load at the top, according to the hyperbolic sine ZZ theory, for several values of p.

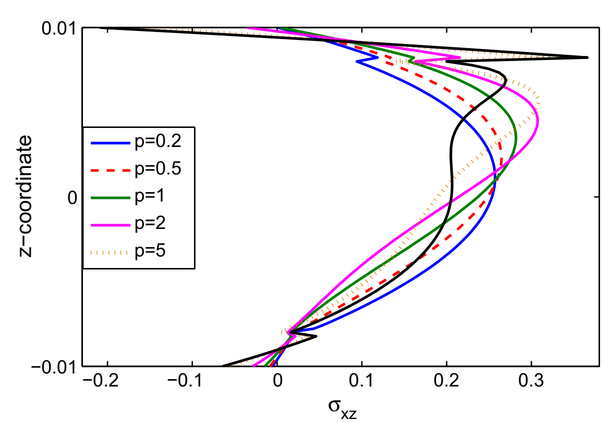

Fig. 11. $\bar{\sigma}_{xz}$ through the thickness direction of a SSSS sandwich square plate with FG core, $a/h = 100$, subjected to sinusoidal load at the top, according to the hyperbolic sine ZZ theory, for several values of p.

6.2. Sandwich with FG skins

We now focus on sandwich plates with isotropic core and FG skins. All examples consider a sandwich plate made of aluminum (55) and zirconia (54) and with side-to-thickness ratio $a/h = 10$. Ta-

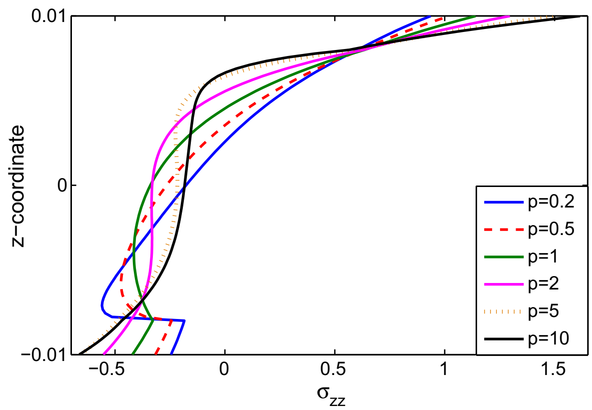

Fig. 12. $\bar{\sigma}_{zz}$ through the thickness direction of a SSSS sandwich square plate with FG core, $a/h = 100$, subjected to sinusoidal load at the top, according to the hyperbolic sine ZZ theory, for several values of p.

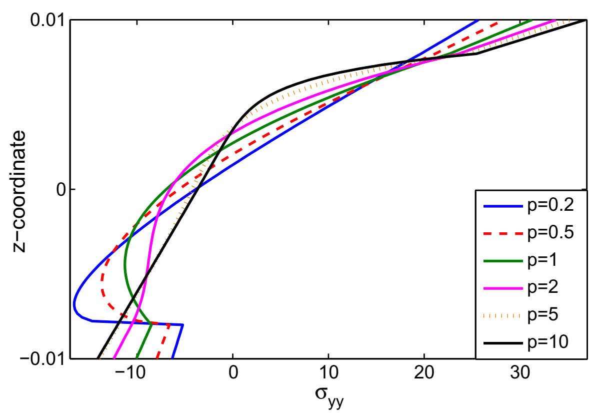

Fig. 13. $\bar{\sigma}_{yy}$ through the thickness direction of a SSSS sandwich square plate with FG core, $a/h = 100$, subjected to sinusoidal load at the top, according to the hyperbolic sine ZZ theory, for several values of p.

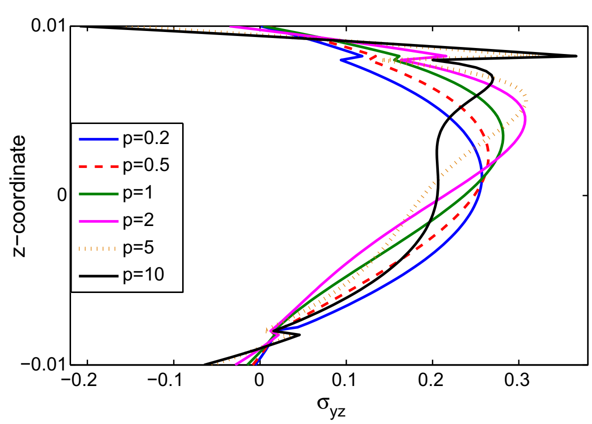

Fig. 14. $\bar{\sigma}_{yz}$ through the thickness direction of a SSSS sandwich square plate with FG core, $a/h = 100$, subjected to sinusoidal load at the top, according to the hyperbolic sine ZZ theory, for several values of p.

Table 9
Convergence study for a 2-1-2 sandwich with FG skins and $p = 1$.

Grid	11^2	13^2	15^2	17^2	19^2
$\bar{w}(0)$	0.3069	0.3069	0.3070	0.3070	0.3070
$\bar{\sigma}_{xx}$	1.4835	1.4801	1.4813	1.4810	1.4811
$\bar{\sigma}_{xz}$	0.2749	0.2744	0.2745	0.2745	0.2745

bles are organized so that the material power-law exponent increases from up to down ($p = 0$, 0.2, 0.5, 1, 2, 5, 10) and the core thickness to the total thickness of the plate ratio increases from left to right $\left(\frac{h_c}{h} = \frac{1}{5}, \frac{1}{4}, \frac{1}{3}, \frac{2}{5}, \frac{1}{2}\right)$.

The non-dimensional displacements and stresses are given as

$$\begin{aligned}
\bar{w} &= \frac{10hE_0}{a^2 p_z} w, \quad \text{evaluated at the center of the plate} \\
\bar{u} &= \frac{10hE_0^2}{a^2 p_z} u, \quad \text{evaluated at the center of the plate} \\
\bar{\sigma}_{xx} &= \frac{10h^2}{a^2 p_z} \sigma_{xx}, \quad \text{evaluated at the center of theplate} \\
\bar{\sigma}_{xz} &= \frac{h}{a p_z} \sigma_{xz}, \quad \text{evaluated at the midpoint of the side}
\end{aligned} \tag{58}$$

Table 10
Convergence study for a 2-2-1 sandwich with FG skins and $p = 5$.

Grid	11^2	13^2	15^2	17^2	19^2
$\bar{w}(0)$	0.3489	0.3490	0.3490	0.3490	0.3490
$\bar{\sigma}_{xx}$	1.5917	1.5880	1.5893	1.5889	1.5891
$\bar{\sigma}_{xz}$	0.2673	0.2667	0.2669	0.2668	0.2668

Table 11
$\bar{w}(0)$ of a sandwich plate with FG skins, for several exponents p and skin-core-skin ratios.

Source	2-1-2	2-1-1	1-1-1	2-2-1	1-2-1
$p = 0$					
SSDPT	0.19605		0.19605	0.19605	0.19605
TSDPT	0.19606		0.19606	0.19606	0.19606
FSDPT	0.19607		0.19607	0.19607	0.19607
CLPT	0.18560		0.18560	0.18560	0.18560
Present $\epsilon_{zz} = 0$	0.1961	0.1961	0.1961	0.1961	0.1961
Present $\epsilon_{zz} \neq 0$	0.1949	0.1949	0.1949	0.1949	0.1949
$p = 0.2$					
Present $\epsilon_{zz} = 0$	0.2312	0.2290	0.2276	0.2249	0.2223
Present $\epsilon_{zz} \neq 0$	0.2297	0.2275	0.2261	0.2235	0.2209
$p = 0.5$					
Present $\epsilon_{zz} = 0$	0.2667	0.2614	0.2583	0.2519	0.2460
Present $\epsilon_{zz} \neq 0$	0.2650	0.2597	0.2566	0.2503	0.2444
$p = 1$					
SSDPT	0.30624		0.29194	0.28082	0.27093
TSDPT	0.30632		0.29199	0.28085	0.27094
FSDPT	0.30750		0.29301	0.28168	0.27167
CLPT	0.29417		0.28026	0.26920	0.25958
Present $\epsilon_{zz} = 0$	0.3090	0.2995	0.2949	0.2838	0.2740
Present $\epsilon_{zz} \neq 0$	0.3070	0.2975	0.2929	0.2820	0.2722
$p = 2$					
SSDPT	0.35218		0.33280	0.31611	0.30260
TSDPT	0.35231		0.33289	0.31617	0.30263
FSDPT	0.35408		0.33441	0.31738	0.30370
CLPT	0.33942		0.32067	0.30405	0.29095
Present $\epsilon_{zz} = 0$	0.3542	0.3399	0.3351	0.3186	0.3053
Present $\epsilon_{zz} \neq 0$	0.3519	0.3376	0.3329	0.3164	0.3032
$p = 5$					
SSDPT	0.39160		0.37128	0.34950	0.33474
TSDPT	0.39183		0.37145	0.34960	0.33480
FSDPT	0.39418		0.37356	0.35123	0.33631
CLPT	0.37789		0.35865	0.33693	0.32283
Present $\epsilon_{zz} = 0$	0.3930	0.3746	0.3729	0.3514	0.3370
Present $\epsilon_{zz} \neq 0$	0.3905	0.3722	0.3705	0.3490	0.3347
$p = 10$					
SSDPT	0.40376		0.38490	0.34916	0.34119
TSDPT	0.40407		0.38551	0.36215	0.34824
FSDPT	0.40657		0.38787	0.36395	0.34996
CLPT	0.38941		0.37236	0.34915	0.33612
Present $\epsilon_{zz} = 0$	0.4051	0.3861	0.3868	0.3637	0.3503
Present $\epsilon_{zz} \neq 0$	0.4026	0.3835	0.3843	0.3612	0.3480

Two convergence studies were performed, varying the exponent power-law p and the symmetry of the sandwich. Table 9 refers to the symmetric 2-1-2 plate with $p = 1$ and Table 10 refers to the non-symmetric 2-2-1 plate with $p = 5$. A 15^2 grid was chosen for the following static problems.

Results refering to the displacements of a sandwich plate with FG skins are presented in Table 11 and Figs. 15–17. In Table 11, the transverse displacement are tabulated and compared with available references, for several values of p and skin-core-skin thickness ratios. In Fig. 15, the influence of the thickness-stretching on the deformed of the symmetric 1-2-1 simply supported sandwich square plate with FG skins, with $p = 10$, subjected to sinusoidal load at the top, is visualized. Fig. 15 is the plot of the bottom ($z = -h/2$) of the plate. In Figs. 16 and 17 the influence of the

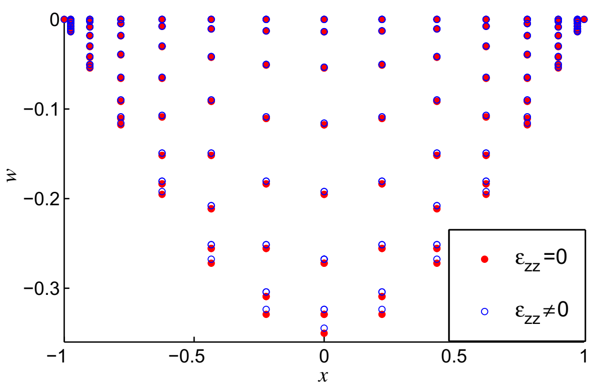

Fig. 15. Deformed of the SSSS 1-2-1 sandwich square plate with FG skins, $p = 10$, subjected to sinusoidal load at the top, according to the hyperbolic sine ZZ theory, considering and disregarding thickness-stretching.

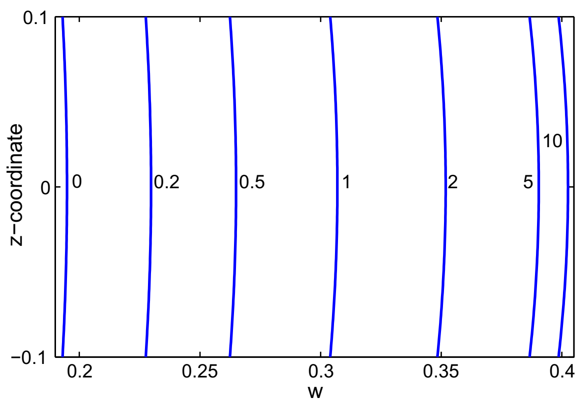

Fig. 16. Out-of-plane displacement through the thickness of the SSSS 2-1-2 sandwich square plate with FG skins, subjected to sinusoidal load at the top, according to the hyperbolic sine ZZ theory, for various values of p.

Table 12
$\bar{\sigma}_{xx}(h/2)$ of a sandwich plate with FG skins, for several exponents p and skin-core-skin ratios.

Source	2-1-2	2-1-1	1-1-1	2-2-1	1-2-1
$p = 0$					
SSDPT	2.05452		2.05452	2.05452	2.05452
TSDPT	2.04985		2.04985	2.04985	2.04985
FSDPT	1.97576		1.97576	1.97576	1.97576
Present $\epsilon_{zz} = 0$	1.9947	1.9945	1.9947	1.9946	1.9946
Present $\epsilon_{zz} \neq 0$	2.0066	2.0064	2.0066	2.0065	2.0064
$p = 0.2$					
Present $\epsilon_{zz} = 0$	1.0962	1.0705	1.0795	1.0526	1.0533
Present $\epsilon_{zz} \neq 0$	1.1024	1.0767	1.0857	1.0587	1.0595
$p = 0.5$					
Present $\epsilon_{zz} = 0$	1.2690	1.2088	1.2285	1.1679	1.1694
Present $\epsilon_{zz} \neq 0$	1.2757	1.2153	1.2351	1.1743	1.1759
$p = 1$					
SSDPT	1.49859		1.42892	1.32342	1.32590
TSDPT	1.49587		1.42617	1.32062	1.32309
FSDPT	1.45167		1.38303	1.27749	1.28096
Present $\epsilon_{zz} = 0$	1.4742	1.3700	1.4067	1.3026	1.3064
Present $\epsilon_{zz} \neq 0$	1.4813	1.3768	1.4137	1.3092	1.3133
$p = 2$					
SSDPT	1.72412		1.63025	1.47387	1.48283
TSDPT	1.72144		1.62748	1.47095	1.47988
FSDPT	1.67496		1.58242	1.42528	1.43580
Present $\epsilon_{zz} = 0$	1.6920	1.5386	1.6017	1.4476	1.4588
Present $\epsilon_{zz} \neq 0$	1.6994	1.5456	1.6088	1.4543	1.4659
$p = 5$					
SSDPT	1.91547		1.81838	1.61477	1.64106
TSDPT	1.91302		1.81580	1.61181	1.63814
FSDPT	1.86479		1.76988	1.56401	1.59309
Present $\epsilon_{zz} = 0$	1.8761	1.6836	1.7833	1.5826	1.6123
Present $\epsilon_{zz} \neq 0$	1.8838	1.6909	1.7906	1.5893	1.6195
$p = 10$					
SSDPT	1.97313		1.88147	1.61979	1.64851
TSDPT	1.97126		1.88376	1.66660	1.70417
FSDPT	1.92165		1.83754	1.61645	1.65844
Present $\epsilon_{zz} = 0$	1.9316	1.7328	1.8485	1.6327	1.6761
Present $\epsilon_{zz} \neq 0$	1.9397	1.7405	1.8559	1.6395	1.6832

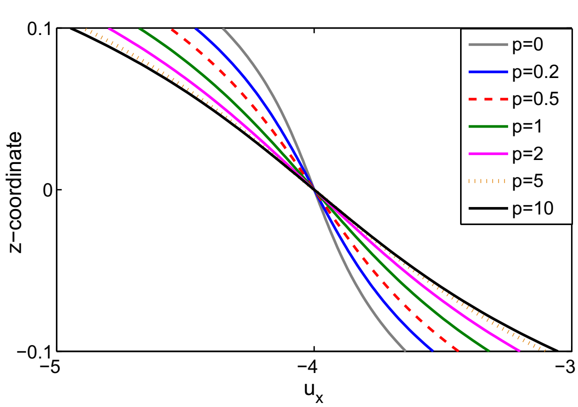

Fig. 17. In-plane displacement through the thickness of the SSSS 2-1-2 sandwich square plate with FG skins, subjected to sinusoidal load at the top, according to the hyperbolic sine ZZ theory, for various values of p.

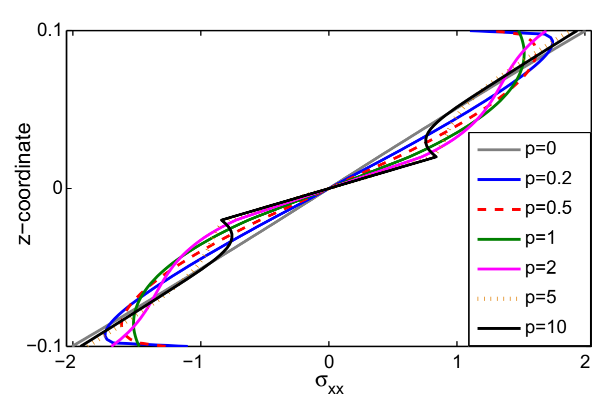

Fig. 18. $\bar{\sigma}_{xx}$ through the thickness of the SSSS 2-1-2 sandwich square plate with FG skins, subjected to sinusoidal load at the top, according to the hyperbolic sine ZZ theory, for various values of p.

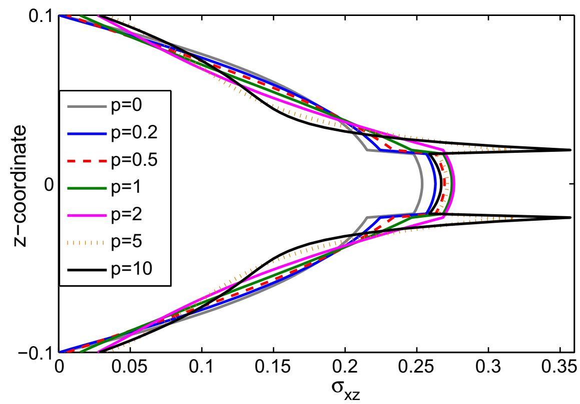

Fig. 19. $\bar{\sigma}_{xz}$ through the thickness of the SSSS 2-1-2 sandwich square plate with FG skins, subjected to sinusoidal load at the top, according to the hyperbolic sine ZZ theory, for various values of *p*.

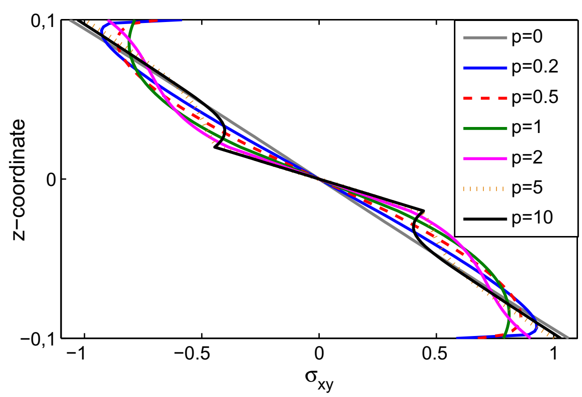

Fig. 20. $\bar{\sigma}_{xy}$ through the thickness of the SSSS 2-1-2 sandwich square plate with FG skins, subjected to sinusoidal load at the top, according to the hyperbolic sine ZZ theory, for various values of *p*.

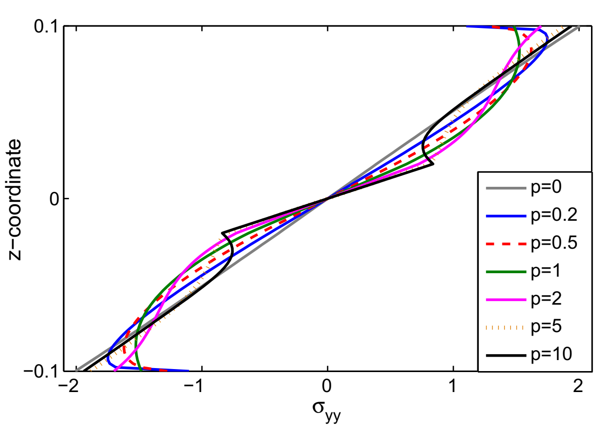

Fig. 21. $\bar{\sigma}_{yy}$ through the thickness of the SSSS 2-1-2 sandwich square plate with FG skins, subjected to sinusoidal load at the top, according to the hyperbolic sine ZZ theory, for various values of *p*.

power-law exponent *p* in the displacements u_x and *w*, respectively, can be visualized. The figures refer to the simply supported 2-1-2 sandwich square plate with FG skins, subjected to sinusoidal load at the top, and presents the displacements through the thickness, according to the hyperbolic sine ZZ theory, for various values of *p*.

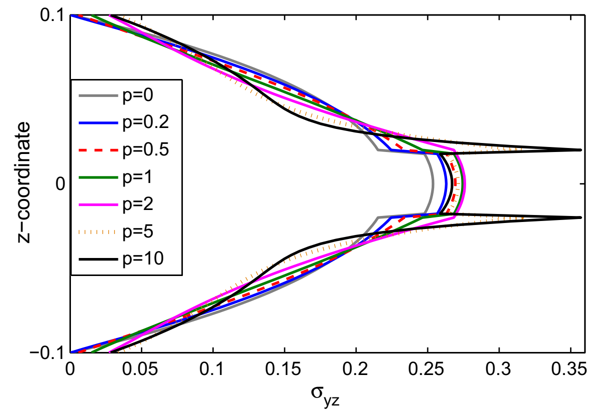

Fig. 22. $\bar{\sigma}_{yz}$ through the thickness of the SSSS 2-1-2 sandwich square plate with FG skins, subjected to sinusoidal load at the top, according to the hyperbolic sine ZZ theory, for various values of *p*.

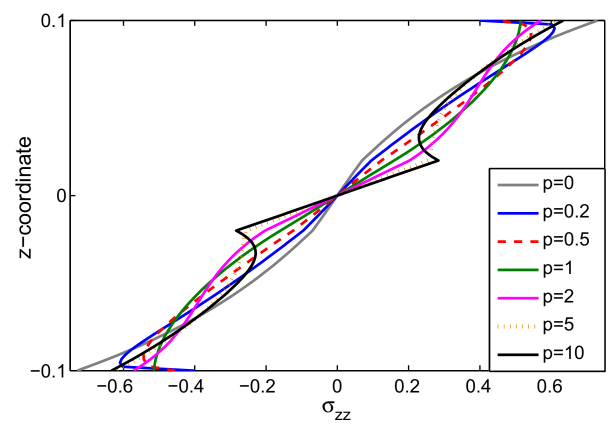

Fig. 23. $\bar{\sigma}_{zz}$ through the thickness of the SSSS 2-1-2 sandwich square plate with FG skins, subjected to sinusoidal load at the top, according to the hyperbolic sine ZZ theory, for various values of *p*.

The deflection of a simply supported sandwich plate with FG skins increases as the power-law of the material increases. This is seen in Table 11 for all studied plates and in Fig. 16 for a particular one. As the core thickness to the plate thickness ratio increases, the transverse displacement decreases. The results depend on the ϵ_{zz} approach.

Table 12 and Fig. 18 present results refering to $\bar{\sigma}_{xx}$. The values obtained with present hyperbolic sine ZZ theory and RBF collocation are tabulated in Table 12 and compared with available references, for various *p* and skin-core-skin thickness ratios. Fig. 18 shows the stress through the thickness for the simply supported 2-1-2 sandwich square plate with FG skins, subjected to sinusoidal load at the top, for various values of *p* (see Figs. 19–23).

In all tables, a good agreement between the present solution and references considered is obtained. (See Table 13).

7. Conclusions

In this paper we presented a study using the radial basis function collocation method to analyze static deformations of thin and thick functionally graded sandwich plates using a variation of Murakami's Zig-Zag function, considering a hyperbolic sine term for the in-plane displacement expansion and allowing for through-the-thickness deformations. This has not been done before and serves to fill the gap of knowledge in this area.

Table 13
$\bar{\sigma}_{xz}(0)$ of a sandwich plate with FG skins, for several exponents p and skin-core-skin ratios.

Source	2-1-2	2-1-1	1-1-1	2-2-1	1-2-1
$p = 0$					
SSDPT	0.24618		0.24618	0.24618	0.24618
TSDPT	0.23857		0.23857	0.23857	0.23857
FSDPT	0.19099		0.19099	0.19099	0.19099
Present $\epsilon_{zz} = 0$	0.2538	0.2284	0.2459	0.2407	0.2358
Present $\epsilon_{zz} \neq 0$	0.2538	0.2291	0.2461	0.2411	0.2363
$p = 0.2$					
Present $\epsilon_{zz} = 0$	0.2629	0.2388	0.2539	0.2483	0.2419
Present $\epsilon_{zz} \neq 0$	0.2630	0.2396	0.2541	0.2488	0.2424
$p = 0.5$					
Present $\epsilon_{zz} = 0$	0.2693	0.2489	0.2593	0.2537	0.2455
Present $\epsilon_{zz} \neq 0$	0.2694	0.2498	0.2595	0.2542	0.2461
$p = 1$					
SSDPT	0.27774		0.26809	0.26680	0.26004
TSDPT	0.27104		0.26117	0.25951	0.25258
FSDPT	0.24316		0.23257	0.22762	0.22057
Present $\epsilon_{zz} = 0$	0.2744	0.2630	0.2640	0.2590	0.2489
Present $\epsilon_{zz} \neq 0$	0.2745	0.2640	0.2643	0.2594	0.2496
$p = 2$					
SSDPT	0.29422		0.27807	0.27627	0.26543
TSDPT	0.28838		0.27188	0.26939	0.25834
FSDPT	0.26752		0.25077	0.24316	0.23257
Present $\epsilon_{zz} = 0$	0.2758	0.2866	0.2664	0.2632	0.2515
Present $\epsilon_{zz} \neq 0$	0.2760	0.2877	0.2668	0.2636	0.2523
$p = 5$					
SSDPT	0.31930		0.29150	0.28895	0.27153
TSDPT	0.31454		0.28643	0.28265	0.26512
FSDPT	0.29731		0.27206	0.26099	0.24596
Present $\epsilon_{zz} = 0$	0.2710	0.3367	0.2651	0.2666	0.2538
Present $\epsilon_{zz} \neq 0$	0.2712	0.3377	0.2655	0.2669	0.2546
$p = 10$					
SSDPT	0.33644		0.29529	0.29671	0.27676
TSDPT	0.33242		0.29566	0.29080	0.26895
FSDPT	0.31316		0.28299	0.26998	0.25257
Present $\epsilon_{zz} = 0$	0.2669	0.3795	0.2635	0.2690	0.2559
Present $\epsilon_{zz} \neq 0$	0.2671	0.3806	0.2639	0.2692	0.2568

Using the Unified Formulation, the plate formulation was easily discretized by radial basis functions collocation. The hardworking of deriving the equations of motion and boundary conditions is eliminated with the present approach. The combination of Carrera's Unified Formulation and collocation with RBFs proved to be a simple yet powerful alternative to other finite element or meshless methods in the static deformation of thin and thick functionally graded sandwich plates.

Numerical examples were performed on simply supported sandwich plates, made of functionally graded materials in the core or in the skins, for various material power-law exponents and side-to-thickness and skin-core-skin thickness ratios. Obtained results were presented in figures and tables and compared with references and these demonstrate the accuracy of present approach.

Allow or not extensibility in the thickness direction has influence on the obtained results, more significatively in thicker plates. The σ_{zz} should be considered in the formulation, even for thinner functionally graded samdwich plates.

Acknowledgements

The first author is grateful for the grant SFRH/BD/45554/2008 assured by FCT. The authors thank the financial support of FCT, through POCTI and POCI (2010)/FEDER. In particular the support to LAETA via project Composites in Mechanical Design and the support to PTDC/EME-PME/120830/2012 is gratefully acknowledged.

References

[1] Kirchhoff G. Uber das gleichgewicht und die bewegung einer elastischen scheibe. J Angew Math 1850;40:51–88.
[2] Reissner E. The effect of transverse shear deformations on the bending of elastic plates. J Appl Mech 1945;12:A69–77.
[3] Mindlin RD. Influence of rotary inertia and shear in flexural motions of isotropic elastic plates. J Appl Mech 1951;18:31–8.
[4] Zenkert D. An introduction to sandwich structures. Oxford: Chamelon Press; 1995.
[5] Vinson JR. The behavior of sandwich structures of isotropic and composite materials. Technomic Publishing Co.; 1999.
[6] Burton S, Noor AK. Assessment of computational model for sandwich panels and shells. Comput Methods Appl Mech Eng 1995;124:125–51.
[7] Noor AK, Burton S, Bert CW. Computational model for sandwich panels and shells. Appl Mech Rev 1996;49:155–99.
[8] Altenbach H. Theories for laminated and sandwich plates. Mech Compos Mater 1998;34:243–52. http://dx.doi.org/10.1007/BF02256043.
[9] Librescu Liviu, Hause Terry. Recent developments in the modeling and behavior of advanced sandwich constructions: a survey. Compos Struct 2000;48(1–3):1–17.
[10] Vinson Jack R. Sandwich structures. Appl Mech Rev 2001;54(3):201–14.
[11] Demasi L. 2D, quasi 3d and 3d exact solutions for bending of thick and thin sandwich plates. J Sandwich Struct Mater 2008;10:271–310.
[12] Carrera E. Historical review of zig-zag theories for multilayered plates and shells. Appl Mech Rev 2003;56:287–308.
[13] Murakami H. Laminated composite plate theory with improved in-plane responses. J Appl Mech 1986;53:661–6.
[14] Carrera E. Developments, ideas, and evaluations based upon reissner's mixed variational theorem in the modelling of multilayered plates and shells. Appl Mech Rev 2001;54:301–29.
[15] Carrera E. The use of murakami's zig-zag function in the modeling of layered plates and shells. Compos Struct 2004;82:541–54.
[16] Demasi L. ∞^3 hierarchy plate theories for thick and thin composite plates: the generalized unified formulation. Compos Struct 2008;84:256–70.
[17] Brischetto S, Carrera E, Demasi L. Improved bending analysis of sandwich plate by using zig-zag function. Compos Struct 2009;89:408–15.
[18] Hon YC, Lu MW, Xue WM, Zhu YM. Multiquadric method for the numerical solution of byphasic mixture model. Appl Math Comput 1997;88:153–75.
[19] Hon YC, Cheung KF, Mao XZ, Kansa EJ. A multiquadric solution for the shallow water equation. ASCE J Hydraul Eng 1999;125(5):524–33.
[20] Wang JG, Liu GR, Lin P. Numerical analysis of biot's consolidation process by radial point interpolation method. Int J Solids Struct 2002;39(6):1557–73.
[21] Liu GR, Gu YT. A local radial point interpolation method (lrpim) for free vibration analyses of 2-d solids. J Sound Vib 2001;246(1):29–46.
[22] Liu GR, Wang JG. A point interpolation meshless method based on radial basis functions. Int J Numer Methods Eng 2002;54:1623–48.
[23] Wang JG, Liu GR. On the optimal shape parameters of radial basis functions used for 2-d meshless methods. Comput Methods Appl Mech Eng 2002;191:2611–30.
[24] Chen XL, Liu GR, Lim SP. An element free galerkin method for the free vibration analysis of composite laminates of complicated shape. Compos Struct 2003;59:279–89.
[25] Dai KY, Liu GR, Lim SP, Chen XL. An element free galerkin method for static and free vibration analysis of shear-deformable laminated composite plates. J Sound Vib 2004;269:633–52.
[26] Liu GR, Chen XL. Buckling of symmetrically laminated composite plates using the element-free galerkin method. Int J Struct Stability Dynam 2002;2:281–94.
[27] Liew KM, Chen XL, Reddy JN. Mesh-free radial basis function method for buckling analysis of non-uniformity loaded arbitrarily shaped shear deformable plates. Comput Methods Appl Mech Eng 2004;193:205–25.
[28] Q Huang Y, Li QS. Bending and buckling analysis of antisymmetric laminates using the moving least square differential quadrature method. Comput Methods Appl Mech Eng 2004;193:3471–92.
[29] Liu L, Liu GR, Tan VCB. Element free method for static and free vibration analysis of spatial thin shell structures. Comput Methods Appl Mech Eng 2002;191:5923–42.
[30] Xiang S, Wang KM, Ai YT, Sha YD, Shi H. Analysis of isotropic, sandwich and laminated plates by a meshless method and various shear deformation theories. Compos Struct 2009;91(1):31–7.
[31] Xiang S, Shi H, Wang KM, Ai YT, Sha YD. Thin plate spline radial basis functions for vibration analysis of clamped laminated composite plates. Eur J Mech A/Solids 2010;29:844–50.
[32] Ferreira AJM. A formulation of the multiquadric radial basis function method for the analysis of laminated composite plates. Compos Struct 2003;59:385–92.
[33] Ferreira AJM. Thick composite beam analysis using a global meshless approximation based on radial basis functions. Mech Adv Mater Struct 2003;10:271–84.
[34] Ferreira AJM, Roque CMC, Martins PALS. Analysis of composite plates using higher-order shear deformation theory and a finite point formulation based on the multiquadric radial basis function method. Composites: Part B 2003;34:627–36.
[35] Carrera E. Evaluation of layer-wise mixed theories for laminated plate analysis. AIAA J 1998(36):830–9.

[36] Carrera Erasmo. Theories and finite elements for multilayered plates and shells: a unified compact formulation with numerical assessment and benchmarking. Arch Comput Methods Eng 2003;10:215–96.
[37] Brischetto S, Carrera E. Advanced mixed theories for bending analysis of functionally graded plates. Comput Struct 2010;88(23–24):1474–83.
[38] Brischetto S. Classical and mixed advanced models for sandwich plates embedding functionally graded cores. J Mech Mater Struct 2009;4:13–33.
[39] Carrera E, Brischetto S, Robaldo A. Variable kinematic model for the analysis of functionally graded material plates. AIAA J 2008;46:194–203.
[40] Ferreira AJM, Roque CMC, Carrera E, Cinefra M, Polit O. Radial basis functions collocation and a unified formulation for bending, vibration and buckling analysis of laminated plates, according to a variation of murakami's zig-zag theory. Eur J Mech – A/Solids 2011;30(4):559–70.
[41] Rodrigues JD, Roque CMC, Ferreira AJM, Carrera E, Cinefra M. Radial basis functions-finite differences collocation and a unified formulation for bending, vibration and buckling analysis of laminated plates, according to murakami's zig-zag theory. Compos Struct 2011;93(7):1613–20.
[42] Ferreira AJM, Roque CMC, Carrera E, Cinefra M, Polit O. Two higher order zig-zag theories for the accurate analysis of bending, vibration and buckling response of laminated plates by radial basis functions collocation and a unified formulation. J Compos Mater 2011;45(24):2523–36.
[43] Neves AMA, Ferreira AJM, Carrera E, Cinefra M, Roque CMC, Jorge RMN, et al. A quasi-3D hyperbolic shear deformation theory for the static and free vibration analysis of functionally graded plates. Compos Struct 2012;94(5):1814–25.
[44] Miyamoto Y, Kaysser WA, Rabin BH, Kawasaki A, Ford RG. Functionally graded materials: design, processing and applications. Kluwer Academic Publishers; 1999.
[45] Jin ZH, Batra RC. Stress intensity relaxation at the tip of an edge crack in a functionally graded material subjected to a thermal shock. J Therm Stress 1996;19:317–39.
[46] Chung YL, Chi SH. The residual stress of functionally graded materials. J Chinese Inst Civil Hydraul Eng 2001;13:1–9.
[47] Praveen GN, Reddy JN. Nonlinear transient thermoelastic analysis of functionally graded ceramic-metal plates. Int J Solids Struct 1998;35(33):4457–76.
[48] Najafizadeh MM, Eslami MR. Buckling analysis of circular plates of functionally graded materials under uniform radial compression. Int J Mech Sci 2002;44(12):2479–93.
[49] Zenkour AM. A comprehensive analysis of functionally graded sandwich plates: part 1 – deflection and stresses. Int J Solids Struct 2005;42(18–19):5224–42.
[50] Zenkour AM. Generalized shear deformation theory for bending analysis of functionally graded plates. Appl Math Modell 2006;30:67–84.
[51] Mori T, Tanaka K. Average stress in matrix and average elastic energy of materials with misfitting inclusions. Acta Metall 1973;21(5):571–4.
[52] Benveniste Y. A new approach to the application of mori-tanaka's theory in composite materials. Mech Mater 1987;6(2):147–57.
[53] Kansa EJ. Multiquadrics – a scattered data approximation scheme with applications to computational fluid dynamics. I: surface approximations and partial derivative estimates. Comput Math Appl 1990;19(8/9):127–45.
[54] Ferreira AJM, Fasshauer GE. Computation of natural frequencies of shear deformable beams and plates by a rbf-pseudospectral method. Comput Methods Appl Mech Eng 2006;196:134–46.
[55] Carrera E, Brischetto S, Cinefra M, Soave M. Effects of thickness stretching in functionally graded plates and shells. Compos Part B: Eng 2011;42:23–133.